Clays and Clay Minerals, Vol. 59, No. 4, 400–415, 2011.

INTERPRETATION OF REFLECTANCE SPECTRA OF CLAY MINERAL-SILICA MIXTURES: IMPLICATIONS FOR MARTIAN CLAY MINERALOGY AT MAWRTH VALLIS

Nancy K. McKeown[1,*,†], Janice L. Bishop[2], Javier Cuadros[3], Stephen Hillier[4], Elena Amador[1], Heather D. Makarewicz[5], Mario Parente[6], and Eli A. Silver[1]

[1] University of California Santa Cruz, Earth and Planetary Sciences, Santa Cruz, CA 95064, USA
[2] SETI Institute, Mountain View, CA 94043, USA
[3] Natural History Museum, Cromwell Road, London SW7 5BD, UK
[4] James Hutton Institute, Craigiebuckler, Aberdeen AB15 8QH, UK
[5] University of Kansas, Electrical Engineering and Computer Science, Lawrence, KS 66045, USA
[6] Stanford University, Electrical Engineering, Stanford, CA 94035, USA

Abstract—The Al-clay-rich rock units at Mawrth Vallis, Mars, have been identified as mixtures of multiple components based on their spectral reflectance properties and the known spectral character of pure clay minerals. In particular, the spectral characteristics associated with the ~2.2 μm feature in Martian reflectance spectra indicate that mixtures of AlOH- and SiOH-bearing minerals are present. The present study investigated the spectral reflectance properties of the following binary mixtures to aid in the interpretation of remotely acquired reflectance spectra of rocks at Mawrth Vallis: kaolinite-opal-A, kaolinite-montmorillonite, montmorillonite-obsidian, montmorillonite-hydrated silica (opal), and glass-illite-smectite (where glass was hydrothermally altered to mixed-layer illite-smectite). The best spectral matches with Martian data from the present study's laboratory experiments are mixtures of montmorillonite and obsidian having ~50% montmorillonite or mixtures of kaolinite and montmorillonite with ~30% kaolinite. For both of these mixtures the maximum inflection point on the long wavelength side of the 2.21 μm absorption feature is shifted to longer wavelengths, and in the case of the kaolinite-montmorillonite mixtures the 2.17 μm absorption found in kaolinite is of similar relative magnitude to that feature as observed in CRISM (Compact Reconnaissance Imaging Spectrometer for Mars) data. The reflectance spectra of clay mixed with opal and of hydrothermally altered glass-illite-smectite did not represent the Martian spectra observed in this region as well. A spectral comparison of linear *vs.* intimate mixtures of kaolinite and montmorillonite indicated that for these sieved samples, the intimate mixtures are very similar to the linear mixtures with the exception of the altered glass-illite-smectite samples. However, the 2.17 μm kaolinite absorption is stronger in the intimate mixtures than in the equivalent linear mixture. Modified Gaussian Modeling of absorption features observed in reflectance spectra of the kaolinite-montmorillonite mixtures indicated a strong correlation between percent kaolinite in the mixture and the ratio of the area of the 2.16 μm band found in kaolinite to the area of the 2.20 μm band found in montmorillonite.

Key Words—CRISM, Mars, Mawrth Vallis, Spectroscopy.

INTRODUCTION

Clay minerals on Mars are nearly always associated with ancient, Noachian-aged terrains (>3.5 Ga; clay detections in younger outcrops have been described by *e.g.* Marzo *et al.*, 2010; Fairén *et al.*, 2010), causing Bibring *et al.* (2006) to name this period of time the "phyllosian." At Mawrth Vallis, Mars, nontronite, montmorillonite, and a kaolin-family mineral are observed in distinct geologic units (Poulet *et al.*, 2005; Bibring *et al.*, 2007; Bishop *et al.*, 2008b; Wray *et al.*, 2008; McKeown *et al.*, 2009; Loizeau *et al.*, 2010; Noe Dobrea *et al.*, 2010). However, some of the reflectance spectra of kaolin-family minerals appear to be mixed with another component: the 2.21 μm absorption feature indicative of AlOH stretching and bending vibrations is broader than in reflectance spectra of pure kaolinite and the spectra exhibit a distinct 1.9 μm H_2O band that is not observed in spectra of pure kaolinite. This 1.9 μm band may be due to the presence of halloysite, though broadening of the AlOH band indicates that another non-kaolin, hydrated component is present. Some reflectance spectra of possible Martian montmorillonite deposits also exhibit broadening of the 2.21 μm band. Laboratory reflectance spectra of intimate mixtures of these minerals are presented here in order to determine which mineral(s) could account for the features observed in CRISM (Compact Reconnaissance Imaging Spectrometer for Mars) data. The present study focuses

* E-mail address of corresponding author:
mckeownn@macewan.ca
† Present address: Physical Sciences, Grant MacEwan University, 10700 – 104 Ave., Edmonton, AB T5J 4S2, Canada
DOI: 10.1346/CCMN.2011.0590404

on the 2.2 μm wavelength region where CRISM spectra exhibit subtle variations in absorption features that have important implications for mineralogy. Variations are also observed in the 1.4 μm region due to OH overtone vibrations, but often these features are too weak in CRISM data for reliable discrimination of bands.

BACKGROUND

Mawrth Vallis

Mawrth Vallis is located at 25ºN, −20ºE at the boundary between the southern highlands and northern lowlands (Figure 1). It is one of the oldest outflow channels on the planet (Scott and Tanaka, 1986; Edgett and Parker, 1997) and the nearby plains contain some of the most extensive clay deposits known on Mars (Poulet *et al.*, 2005; McKeown, 2009; Michalski and Noe Dobrea, 2007; Bishop *et al.*, 2008b; Loizeau *et al.*, 2010; Noe Dobrea *et al.*, 2010). Analyses of OMEGA (Observatoire pour la Minéralogie, l'Eau, les Glaces et l'Activité) and CRISM (Compact Reconnaissance Imaging Spectrometer for Mars) visible-near infrared reflectance (VNIR) data have identified a nontronite-bearing unit overlain by an Al-phyllosilicate-bearing unit containing two subunits – a montmorillonite-bearing zone and a zone containing a kaolin-family mineral. The two zones of this upper unit also contain hydrated silica (Poulet *et al.*, 2005; Bibring *et al.*, 2007; Bishop *et al.*, 2008b; Wray *et al.*, 2008; McKeown *et al.*, 2009; Loizeau *et al.*, 2010; Noe Dobrea *et al.*, 2010). The clay units are capped by a dark, spectrally unremarkable unit that is probably basaltic in composition (Bishop *et al.*, 2008b; McKeown *et al.*, 2009; Loizeau *et al.*, 2010; Noe Dobrea *et al.*, 2010). The present study focuses on evaluating reflectance spectra of mixtures of Al-rich phyllosilicates and Si-OH species in order to better characterize this upper AlOH- and SiOH-bearing unit at Mawrth Vallis.

Spectral mixtures

In remote-sensing spectroscopy, materials can appear mixed in two ways – areally or intimately. Areal (or checkerboard) mixtures, where two (or more) spatially distinct materials are present within a single pixel, combine in a linear fashion at VNIR wavelengths: the resultant reflectance spectrum is a proportional addition of the reflectance spectra of the individual end members weighted by their cross-sectional area. Intimate mixtures occur when two (or more) materials are mixed together over short spatial scales, such as at the scale of grains. The spectra of these mixtures generally do not behave in a linear fashion in the VNIR (*e.g.* Nash and Conel, 1974; Singer, 1981; Mustard and Pieters, 1989) due to factors such as grain size and differential scattering. For example, Nash and Conel (1974) found for mixtures of ilmenite, pyroxene, and plagioclase that ilmenite greatly reduced the overall albedo, that even small amounts of pyroxene produced a 0.9 μm absorption band in the

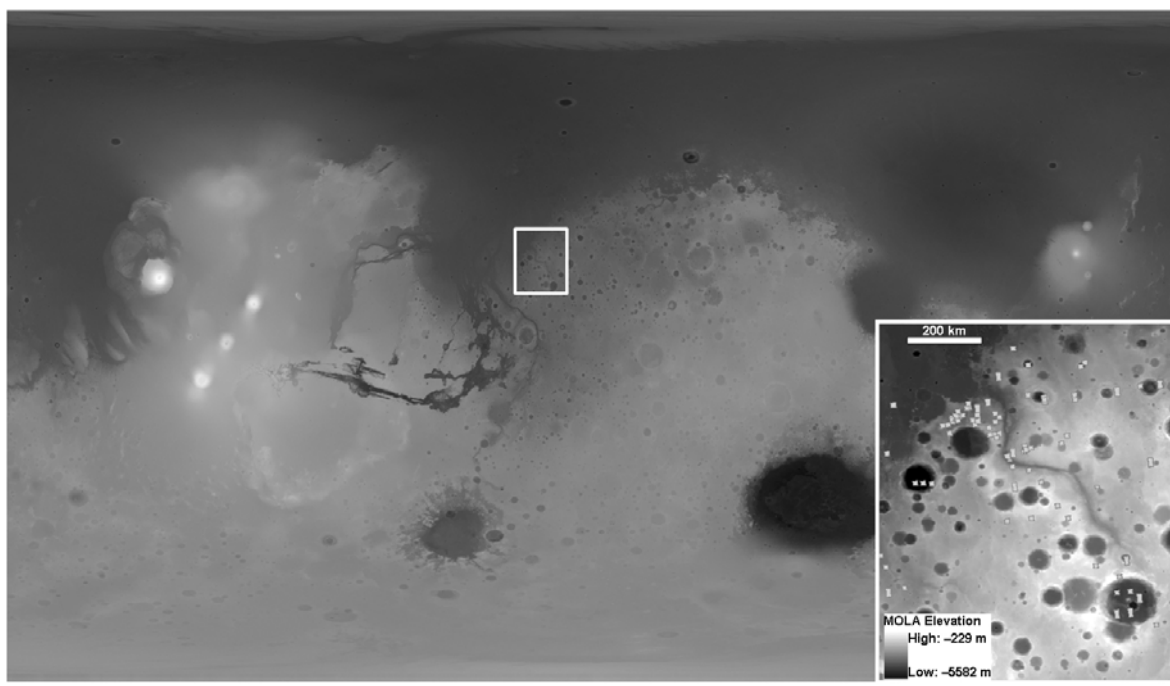

Figure 1. MOLA elevation map of Mars with box showing location of Mawrth Vallis at 25ºN, −20ºE. The inset is an enlargement of the Mawrth Vallis region with regional range of elevations; scale bar = 200 km. The small symbols are CRISM image footprints.

https://doi.org/10.1346/CCMN.2011.0590404 Published online by Cambridge University Press

spectra, and that plagioclase was nearly undetectable at concentrations <75%. Bishop and Dummel (1996) found that for intimate mixtures of ferrihydrite-montmorillonite the reflectance spectra behaved in a non-linear fashion with 5% ferrihydrite, reducing the brightness by as much as 50% at near IR wavelengths.

METHODS

Samples

The kaolinite end member used in the present study was KGa-1 from the Source Clays Repository of The Clay Minerals Society sieved to <125 μm (although the individual particles were finer than this) to remove clumps. The montmorillonite end member used was another source clay, SWy-2, also sieved to <125 μm prior to weighing and mixing (compositions for this and the other samples studied are included in Table 1). The siliceous sample from Kilauea is composed primarily of opal-A and was collected and characterized by Bishop *et al.* (2005) and was ground and sieved to <125 μm. The kaolinite-montmorillonite and kaolinite-opal-A mixtures were prepared under ambient laboratory conditions. Separates were weighed and then mixed together followed by sieving through a <125 μm mesh to ensure homogeneous mixing.

Seven obsidian-montmorillonite samples were prepared in the same way with relative montmorillonite weight proportions of 0, 2 (actual 1.9%), 5 (4.9), 8 (8.2), 10 (9.9), 20 (20.2), 50, 80 (80.2), and 100%. The montmorillonite used in these mixtures was the Al-rich Belle Fourche clay (South Dakota, USA). The obsidian was a sample of rhyolitic composition from Lipari, Italy (Table 1). X-ray diffraction (XRD) analysis of this obsidian showed only silica glass and no sign of alteration minerals. The set of samples containing smectite and either opal-CT or opal-C are naturally occurring bentonites collected by Hillier and Lumsdon (2008) and were characterized by XRD.

The final set of samples was created in the laboratory by hydrothermal alteration of a rhyolitic pumice from Cabo de Gata, Almería, Spain (de la Fuente *et al.*, 2000). Five samples that contain various amounts of mixed-layer illite-smectite (I-S) formed by alteration were examined: 1af with 3.4−6.1% I-S, 7aff with 5.2−6.2% I-S, 12af with 4.8−8.2% I-S, 37af with 6.3% I-S, and 39af with 7.7−8.7% I-S (sample numbers from de la Fuente *et al.*, 2000). The compositions of these samples were determined using XRD (de la Fuente *et al.*, 2002), transmission/analytical electron microscopy (TEM-AEM) (de la Fuente *et al.*, 2002), IR reflectance, and transmission spectroscopy (de la Fuente *et al.*, 2000). The percentages of mixed-layer I-S were determined by Fourier-transform infrared (FTIR) spectroscopy using both diffuse reflectance and transmission modes on samples separated by centrifugation to <2 μm. The reflectance spectra presented here are of the same samples, passed through a 125 μm sieve to homogenize the samples. They are compared to sample ISMt-2 from the Source Clays Repository of The Clay Minerals Society (composition listed in Table 1).

Reflectance spectra

Visible/near-infrared and mid-IR reflectance spectra were measured at the Reflectance Experiment Laboratory (RELAB) at Brown University, Providence, Rhode Island, USA. Bi-directional VNIR spectra from 0.32−2.55 μm were measured relative to Halon under ambient conditions, whereas a Nicolet Nexus 870 FTIR spectrometer equipped with a diffuse reflectance attachment was used to measure off-axis reflectance spectra from 1.0−99.0 μm relative to brushed gold. The samples were measured under H_2O- and CO_2-purged air for the FTIR measurements. Composite, absolute reflectance spectra were

Table 1. Compositions for sample end members.

Sample	Composition
KGa-1	$(Si_{3.85}Al_{0.15})(Al_{3.88}Ti_{0.10}Fe^{3+}_{0.02})(Ca_{0.005}Na_{0.009})\ O_{10}(OH)_8$ [*,†]
SWy-2	$(Si_{7.89}Al_{0.11})(Al_{2.23}Fe^{3+}_{0.42}Mg_{0.56})(Ca_{0.52}Na_{0.14}K_{0.01})\ O_{20}(OH)_4$ [*]
Kilauea silica	(in wt.%) SiO_2 73.67, Al_2O_3 0.52, Fe_2O_3 1.03, MnO <0.01, MgO 0.23, CaO 0.12, Na_2O 0.02, K_2O 0.02, TiO_2 10.15, P_2O_5 0.087, Cr_2O_3 0.142 [‡]
Belle Fourche	$(Si_{7.92}\ Al_{0.08})(Al_{3.12}Fe^{3+}_{0.34}Mg_{0.50}Ti_{0.02})(Na_{0.50}K_{0.02}Ca_{0.06})\ O_{20}(OH)_4$ [Δ]
Obsidian	(in wt.%) SiO_2 76.7, Al_2O_3 12.0, FeO 1.26, K_2O 4.77, Na_2O 3.99, CaO 0.69, TiO_2 0.07, MnO 0.06, MgO 0.04 (total oxide 99.58%) [Δ]
Smectite-opal	Naturally-occurring samples of varying composition [◇]
Rhyolitic pumice	(in wt.%) SiO_2 72.89, Al_2O_3 14.47, Fe_2O_3 1.25, MgO 1.44, CaO 0.86, Na_2O 3.34, K_2O 4.97 [□]
ISMt-2	(in wt.%) SiO_2 50.65, Al_2O_3 25.69, Fe_2O_3 1.94, MnO 0.01, MgO 3.14, CaO 0.21, Na_2O 0.08, K_2O 4.84, TiO_2 0.15, P_2O_5 0.03 [§]

* Mermut and Cano (2001); † Bishop (2002); ‡ Bishop *et al.* (2005); Δ Cuadros (2002); ◇ Hillier and Lumsdon (2008); □ de la Fuente *et al.* (2000); § Vogt *et al.* (2002).

https://doi.org/10.1346/CCMN.2011.0590404 Published online by Cambridge University Press

prepared by scaling and splicing the FTIR data to the bi-directional data near 1.2 μm. The spectral resolution is 5 nm for the bi-directional data and 2–8 cm^{-1} for the FTIR data. Using the reflectance spectra of the pure end members, linear mixture spectra were calculated numerically as an addition of the two end-member spectra weighted by their respective proportions.

Spectral modeling

Modified Gaussian Modeling was performed to characterize the bands in the 2.2 μm wavelength region of the kaolinite-montmorillonite mixtures using techniques described by Sunshine *et al.* (1990) and Sunshine and Pieters (1993), with the exception that a linear spline was used here to define the continuum slope (Makarewicz *et al.*, 2009a). Reflectance values were typically not constant outside of absorption features and needed to be continuum-removed in order to model absorption features as Gaussians properly without the influence of spectral slope affecting the modeled band center, depth, or area. This technique was shown to be successful in identifying components for mixtures of enstatite and clinopyroxene with variable grain sizes (Sunshine and Pieters, 1993). Gaussians have been shown to provide a better fit for reflectance spectra of clays in the OH-stretching region than Lorentzians (*e.g.* Michaelian *et al.*, 1991) and have been used in several studies to model mixtures of clay minerals in laboratory spectra as well as CRISM spectra (Makarewicz *et al.*, 2008, 2009a; Parente *et al.*, 2011).

CRISM data

Full-resolution targeted (FRT) images from the CRISM instrument on the Mars Reconnaissance Orbiter (MRO) consisted of 544 channels covering the spectral range from 0.36 to 3.92 μm at a spectral sampling of 6.5 nm, in ~10–12 km wide swaths at ~18 m/pixel (Murchie *et al.*, 2007). CRISM data were converted to reflectance by subtracting the instrument background, dividing by processed measurements of the internal calibration standard, and dividing by solar irradiance (Murchie *et al.*, 2007, 2009; Mustard *et al.*, 2008). Images are atmospherically corrected using a ratio with an atmospheric transmission spectrum derived from a CRISM scene acquired over the summit of Olympus Mons, scaled to the same column density of CO_2 as discussed by Mustard *et al.* (2008). Images were then processed using a cleaning algorithm to remove noise and large spikes within the data due to instrument effects (Parente, 2008).

Reflectance spectra were retrieved from a 3×3 pixel or 5×5 pixel region of interest and from a similarly sized spectrally unremarkable region (*e.g.* lacking strong absorption features) within the same image (detector) columns. These were then ratioed, with the spectrum of interest in the numerator, to reduce systematic instrument noise (*e.g.* McKeown *et al.*, 2009).

RESULTS: SPECTRAL MIXTURES

The spectral properties of clay-bearing mixtures were evaluated here as multiple sets of binary mixtures. A suite of kaolinite-montmorillonite mixture spectra exhibited variations in brightness and band shape in the VNIR range (Figure 2). Although these spectra were measured under H_2O-purged conditions that should remove the adsorbed H_2O (*e.g.* Bishop *et al.*, 1994), the kaolinite spectrum contains a weak band near 1.95 μm that is attributed to H_2O in minor admixture components of crandallite (1%) in the KGa sample which was identified in XRD by Chipera and Bish (2001). Changes in the band shape were observed in the spectra near 1.4 μm (Figure 2) for the OH-stretching overtone for kaolinite (*e.g.* Petit *et al.*, 1999) and montmorillonite (*e.g.* Bishop *et al.*, 1994) and near 2.16–2.21 μm for the OH combination band (stretch plus bend) in kaolinite and montmorillonite. The present study focuses on the latter region, near 2.2 μm, where CRISM reflectance spectra show subtle variations in spectral character that have important implications for mineralogy.

Kaolinite-montmorillonite

The reflectance spectrum of the pure kaolinite sample exhibited a narrow doublet at 2.17 and 2.21 μm (Figure 3a), consistent with previous studies (*e.g.* Petit *et al.*, 1999; Bishop *et al.*, 2008a). The montmorillonite spectrum has a single absorption at 2.21 μm which is asymmetric toward longer wavelengths (Figure 3a), also consistent with previous studies (*e.g.* Clark *et al.*, 1990; Bishop *et al.*, 1993). All of these features are due to OH vibrations bound to the two Al cations within the di-octahedral sheet of the mineral structure (relatively little Fe or Mg is present in this sample). The differences observed between kaolinite and montmorillonite spectra are due to variations in the OH bonds. For kaolinite, four individual OH absorptions occur between 2.16 and 2.21 μm due to differences in the OH sites (Delineau *et al.*, 1994; Petit *et al.*, 1999). Reflectance spectra of kaolinite-montmorillonite mixtures exhibit changes in the wavelengths of the maximum inflection point on both sides of the ~2.2 μm band. With decreasing kaolinite abundance, the maximum inflection point on the longward side of this absorption shifted to longer wavelengths from 2.23 to 2.27 μm, more similar to montmorillonite (Figure 3). This shift was probably due to a decreased contribution from the kaolinite spectrum, which has a maximum inflection at 2.23 μm, and an increased contribution from the montmorillonite spectrum, which has a maximum inflection at 2.27 μm. The predominance of montmorillonite in this spectral feature is evident with a fairly large percentage of kaolinite still in the mixture (60%) and the inflection point was only shifted by 5 nm from pure montmorillonite when 15% kaolinite was present (Figure 3b). In addition, the absorption at 2.17 μm was reduced as the amount of

https://doi.org/10.1346/CCMN.2011.0590404 Published online by Cambridge University Press

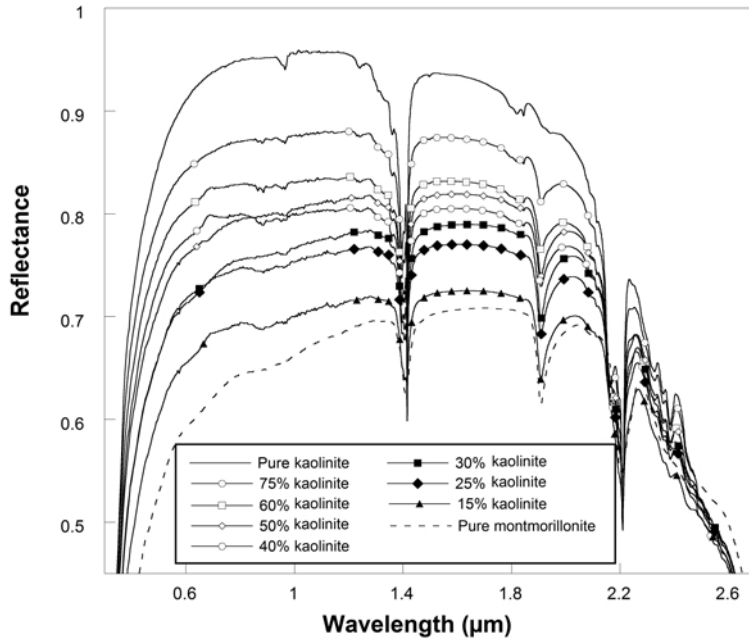

Figure 2. Spectrum of kaolinite-montmorillonite mixtures from 0.3 to 2.6 μm. The brightness increased with increasing amounts of kaolinite in the 0.3−2.1 μm region. The differences are more subtle in the >2.1 μm region and are shown in more detail in Figure 3.

kaolinite decreased. At 60 wt.% kaolinite this feature occurred as a distinct shoulder, whereas at 50 wt.% it occurred as a more gradual shoulder, and at 25 wt.% it was barely detectable (Figure 3a). The band center occurred at 2.209 μm in all mixture spectra as both minerals have a strong absorption at this wavelength.

The effects of intimate mixtures on the reflectance spectra were compared with the effects of linear mixtures in order to evaluate the differences in spectral character expected for rocks on Mars which contain kaolinite and montmorillinite mixed at the grain level *vs.* separate, small outcrops of kaolinite and montmorillonite below the size of CRISM pixels. Comparing the linear (numerical) mixture spectra to spectra of physical mixtures (Figure 3a), the 2.17 μm feature is stronger in spectra of the intimate (physical) mixtures compared to those of the linear mixtures at equivalent phase abundances, suggesting that a simple linear mixing model cannot properly account for spectral variations of intimate mixtures. For shorter wavelengths (0.3−2 μm, *e.g.* Figure 2), the intimate mixture spectra appeared to behave in an approximately linear fashion. Given this similarity, weight percent mixtures were assumed here to have been approximately equivalent to volume percent mixtures, especially as both materials have very similar densities and are finely ground white powders, limiting any differences due to differential scattering.

Kaolinite-Opal-A

The opal-A sample exhibited an asymmetrical absorption centered at 2.21 μm (Figure 4) due to Si−OH vibrations. With lesser amounts of kaolinite in the kaolinite-opal-A mixtures, the absorption at 2.17 μm was reduced but still distinctive down to 30 wt.% kaolinite. At 25 wt.% kaolinite the 2.17 μm absorption was a shoulder on the stronger 2.21 μm absorption (Figure 4). Due to the asymmetric nature of the SiOH absorption, kaolinite band depth was reduced on the longward side of the 2.21 μm feature but was not broadened. Many of the smaller absorption bands in kaolinite in the 2.3−2.4 μm region were reduced in strength as the amount of kaolinite decreased. On the short wavelength side of the kaolinite doublet, the addition of a ~1.9 μm hydration band (not seen in Figure 4) due to opal made the slope from 2 to 2.1 μm flatter rather than negative.

Montmorillonite-obsidian.

Reflectance spectra of montmorillonite exhibited an absorption band centered near 2.209 μm due to Al_2OH (described above) and obsidian spectra had a broader band centered at 2.216 μm due to SiOH stretching and bending vibrations (similar to the SiOH described above); therefore, the center of this band in reflectance spectra of these mixtures did not shift greatly (Figure 5a). The absorption at 2.21 μm was still more characteristic of montmorillonite in the 50-50 mixture, but was much broader and less than half as intense at 20 wt.% montmorillonite.

However, because the obsidian feature was broader, the maximum inflection point on the long wavelength side of the band shifted to longer wavelengths (the 2.21 μm band broadens asymmetrically) with increasing

https://doi.org/10.1346/CCMN.2011.0590404 Published online by Cambridge University Press

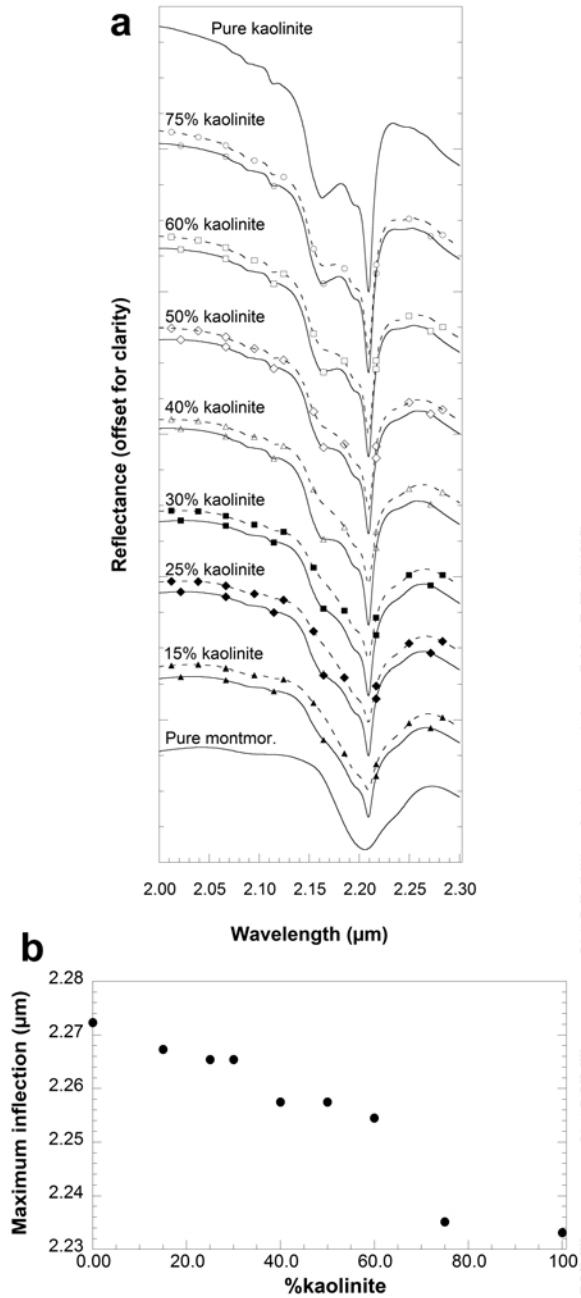

Figure 3. (a) Spectra of linear (calculated spectra, dashed lines) and intimate (physical mixtures, solid lines) mixtures of kaolinite and montmorillonite. In the intimate mixtures (solid lines), the 2.17 μm feature is a distinct absorption down to 50% kaolinite, then is detectable as a strong shoulder down to 30%, a weak shoulder at 25%, and is undetectable at 15% kaolinite. The band strength is slightly reduced and broadened to longer wavelengths with decreasing kaolinite. Comparing the linear and intimate mixtures, the 2.17 μm band is consistently stronger in the intimate mixtures than in the equivalent linear mixtures. Additionally, the maximum inflection point on the longward side shifts from 2.23 μm (pure kaolinite) to 2.26 μm at 40–50% kaolinite, more consistent with montmorillonite. (b) Wavelength of the maximum inflection point longward of 2.21 μm plotted against percent kaolinite in the mixture.

amounts of obsidian. The spectrum of 100% montmorillonite had a maximum inflection point at 2.272 μm. At 50 wt.% montmorillonite the maximum inflection had shifted slightly to 2.276 μm, but was not as sharp as pure montmorillonite (Figure 5). At 20 wt.% the maximum inflection point had shifted to 2.287 μm, a shift that should be detectable in CRISM data. At 10 wt.%, the inflection point jumped to 2.335 μm, indicating a stronger spectral influence of the obsidian; at 8 wt.% montmorillonite, it was at 2.348 μm; and at 5 wt.% the maximum inflection point was very nearly in the same position as pure obsidian (2.362 μm *vs*. 2.368 μm for pure obsidian). The maximum inflection point for the spectrum of 2 wt.% montmorillonite was at a shorter wavelength – 2.357 μm – but the spectra of both 2 wt.%

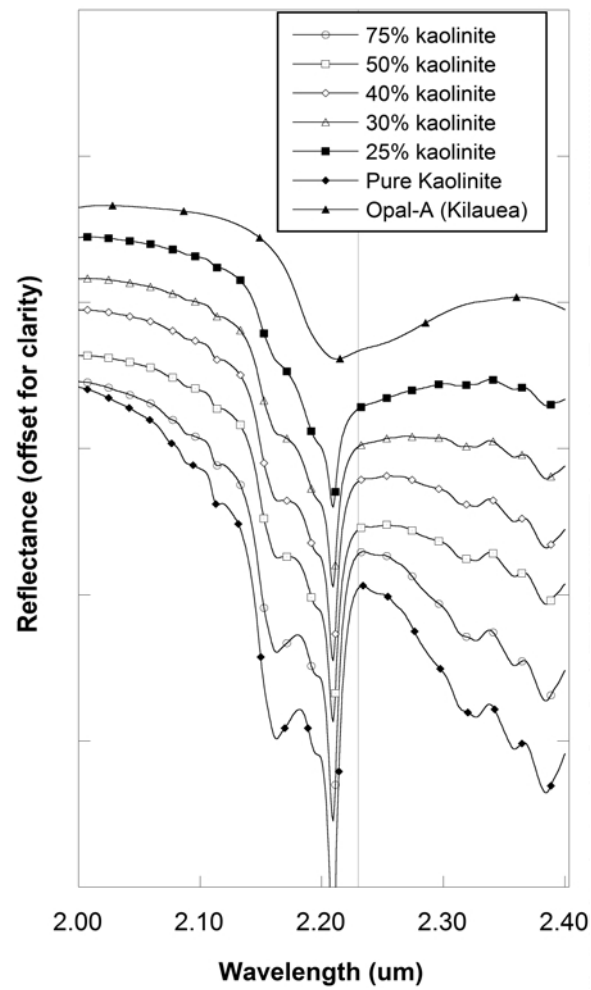

Figure 4. Spectra of kaolinite-opal-A mixtures from 2.0 to 2.4 μm. The band strength longward of 2.21 μm is greatly reduced with increasing opal. The 2.17 μm band is detectable down to 30% kaolinite. The line indicates the inflection point due to kaolinite that did not shift, although the spectral continuum at longer wavelengths increased with increasing opal-A.

https://doi.org/10.1346/CCMN.2011.0590404 Published online by Cambridge University Press

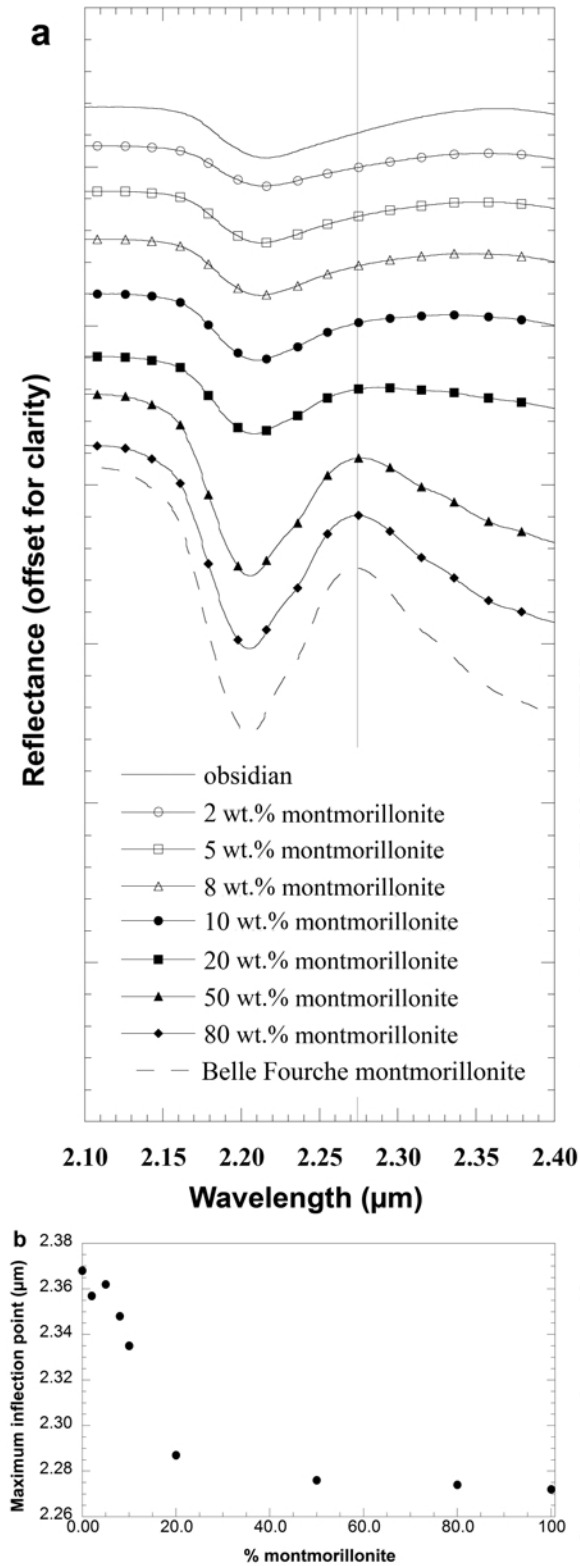

Figure 5. (a) Mixtures of montmorillonite and obsidian from 2.1 to 2.4 μm. At 50%, the spectrum is dominated by montmorillonite, at 20% montmorillonite the 2.21 μm band strength was reduced by more than half and it was broadened slightly to longer wavelengths; by 5% montmorillonite the spectrum was almost identical to that of obsidian. The vertical line marks the maximum inflection point of pure montmorillonite near 2.27 μm. (b) Plot of maximum inflection point *vs*. percent montmorillonite. A distinct shift occurs between 30% and 25% montmorillonite from values near 2.27–2.28 μm to values >2.33 μm.

and 5 wt.% montmorillonite were very flat in this region, and the next highest reflectance value of the 2 wt.% montmorillonite spectrum in this region was at 2.362 μm, the same as the 5 wt.% mixture (Figure 5b).

Opal-montmorillonite

The natural bentonite samples of Hillier and Lumsdon (2008) were comparable to the previous montmorillonite-opal-A physical laboratory mixtures because non-crystalline silica tetrahedra are a major component. This series of bentonites showed that when ⩾50% montmorillonite is present the reflectance spectra exhibited characteristics of montmorillonite and little broadening of the 2.21 μm band due to the presence of opal was observed (Figure 6a). However, the samples with >70% montmorillonite had spectra with a band center at 2.210–2.213 μm, whereas the spectra of samples with smaller amounts of montmorillonite had a band center at 2.207–2.209 μm (Figure 6b). Ongoing Gaussian analyses may help resolve these features. Small differences in band depth at ~2.2 μm were detectable, especially when scaled to the band depth of the montmorillonite spectrum (Table 2).

Hydrothermally altered glass-I-S

The glass-illite-smectite samples, altered in controlled conditions in the laboratory, were again similar to the montmorillonite-opal-A samples (although they contain no opal). They contained very small amounts of mixed-layer illite-smectite (no more than 8.7%; de la Fuente *et al.*, 2000); however, this is enough to substantially change the spectral character in the 2.2 μm region (Figure 7a). The reflectance spectra of the samples containing <6% I-S[1] were essentially unchanged from those of the initial glass, and they exhibited a broad shallow absorption centered at 2.23 μm. Milliken *et al.* (2008) found that reflectance spectra of unaltered hydrated volcanic glasses had an SiOH absorption band at longer wavelengths (2.23 μm) than spectra of

[1] For all but one sample, a range of percent I-S was given due to different results from diffuse reflectance and transmission FTIR. In this discussion, the lowest value was used *e.g.* "<6% I-S" means that the lowest measured value was <6%.

https://doi.org/10.1346/CCMN.2011.0590404 Published online by Cambridge University Press

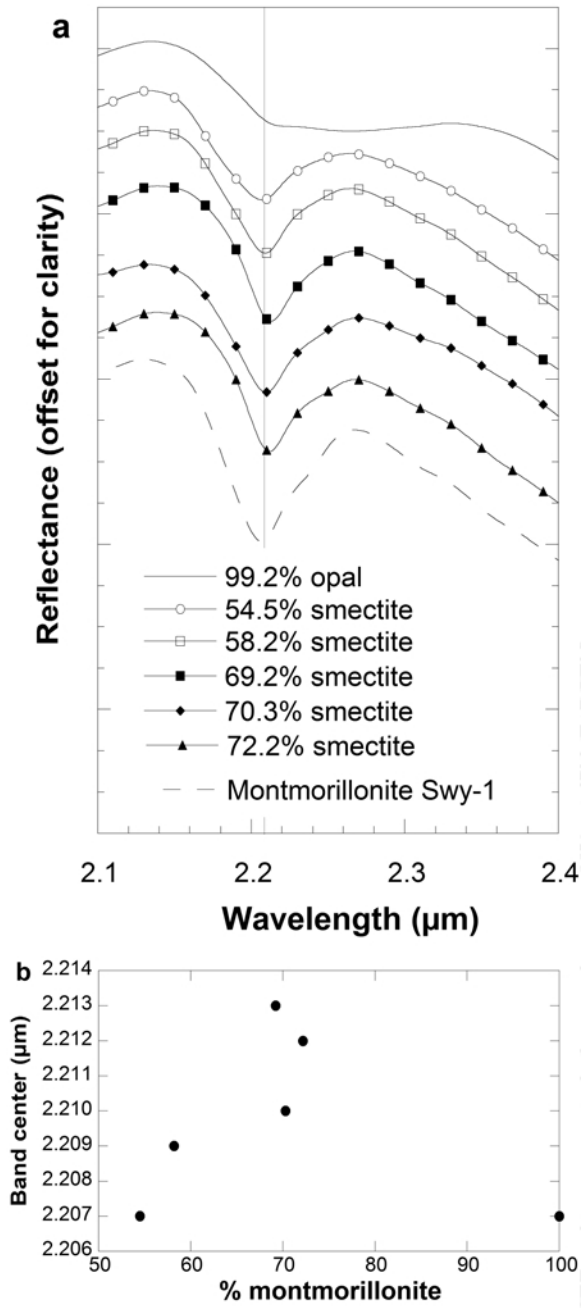

Figure 6. (a) Spectra of opal-smectite natural samples. Most were dominated by montmorillonite, but at 54.5% smectite some broadening of the band was visible on both the longer and shorter wavelengths. The pure montmorillonite spectrum shown here was the SWy-1 standard to provide an example end member. (b) Plot of the 2.21 μm band center *vs*. the percent montmorillonite in the sample.

volcanic glasses that were hydrated due to alteration (*e.g.* opaline weathering rinds; feature at ~2.21 μm). The spectra of samples with 6–8.7% I-S have a much stronger absorption feature centered at 2.23 μm. This stronger band was reminiscent of the 2.21 μm feature in the I-S spectrum but occurred at a slightly longer wavelength and was broader than the feature in the I-S spectrum, probably due to the large amounts of the original silica glass still present in those samples (Figure 7a).

Table 2. Band depths of the 2.21 μm feature in the opal-smectite natural samples in reflectance and the relative percentage of the pure montmorillonite band depth[1].

	Band depth at 2.21 μm (reflectance)	% strength of pure montmorillonite
99.2% opal	0.0639	37.23
54.5% smectite	0.0915	53.36
58.2% smectite	0.1086	63.27
69.2% smectite	0.1182	68.92
70.3% smectite	0.1173	68.35
72.2% smectite	0.1223	71.29
Montmorillonite	0.1716	100.00

[1] The scaled values appear to follow closely the percentage of montmorillonite in the mixture, down to at least 50%.

Unlike the other mixtures presented here, significant differences were observed in the spectra at both longer and shorter wavelengths with increased I-S abundance (Figure 7b,c). In the two samples with >6% I-S (solid symbols on Figure 7), the 1.4 and 1.9 μm features due to H_2O stretching and bending vibration overtones and combinations were stronger than in the other samples (Figure 7b). Additionally, a weak, sharp absorption due to water was present at 1.15 μm and a broad absorption due to electronic transitions of Fe^{3+} was present at 0.95 μm (Burns, 1993). In the samples with <6% I-S, a broad feature was observed centered at 1.14 μm due to electronic transitions of Fe^{2+} (Burns, 1993). Thus, the band shifted due to the presence of greater Fe^{2+} in the samples with less I-S to greater Fe^{3+} in the samples with more I-S. The continuum shape for <6% I-S samples is relatively flat, whereas for the >6% I-S samples, the continuum was convex, with a strong drop off toward the strong 3 μm water feature that is consistent with highly hydrated samples (Figure 7b). Differences were also observed in the shape of the 3 μm 'hydration' feature. In the <6% I-S samples, the feature had relatively straight sides and returned to almost the same level of reflectance as at 2.5 μm (Figure 7c). In the two samples with >6% I-S, the 3 μm feature had a much more gradual rise on the long wavelength side due to additional water in the sample, creating additional absorptions in this area, similar to the shoulder of the I-S spectrum at 3.0 μm (Figure 7c). In addition, the reflectance value on the long wavelength side only returns to ~60% of the reflectance at 2.5 μm. The strength and shape of the 3, 1.9, and 1.4 μm water absorption bands and the presence of a 1.15 μm band indicated that the samples with more I-S were much more hydrated than the samples with less I-S.

https://doi.org/10.1346/CCMN.2011.0590404 Published online by Cambridge University Press

RESULTS: GAUSSIAN MODELING

Modified Gaussian Modeling (MGM) of the 2.2 μm band in reflectance spectra of kaolinite-montmorillonite mixtures identified four bands (Figure 8a): one due exclusively to kaolinite (band 1, centered at 2.16 μm), two due to both kaolinite and montmorillonite (band 2: 2.20 μm and band 3: 2.21 μm), and one due exclusively to montmorillonite (band 4, centered at 2.24 μm). The number, position, and magnitude of these bands were all determined by the modeling algorithm. First, the spectral continuum slope across the absorption feature of interest was determined by the algorithm and removed. Next, the number, position, and magnitude of Gaussian curves required to fit the absorption(s) were determined by the algorithm (Makarewicz *et al.*, 2009b). The four bands identified in the present study were, therefore, not predetermined or constrained in number, position, or magnitude. However, they show remarkable consistency in Gaussian band position and number, with only magnitude varying significantly (Table 3, SOM 1–6. Plots of the MGM results for the linear mixtures are available in SOM 7–15[1]). The area of each band was also calculated and in this case was a better measure of the contribution of that band to the overall spectrum than simple band strength (magnitude).

As the amount of kaolinite decreased, the ratio of the area of band 1 to the area of band 2 decreased linearly (Figure 8b). The same was true of the ratio of the area of band 1 to the sum of the areas of bands 2, 3, and 4 (Figure 8c). The ratio values for the linear mixtures were consistently larger than for the intimate mixtures, as demonstrated by dividing the intimate mixture ratio by the linear mixture ratio (Figure 8d), indicating that the 2.16 μm band was stronger in the numerical linear mixtures than the intimate mixtures. However, the numerical models of the linear mixture spectra with >50% kaolinite have band area ratios which were closer to each other (ratio >0.65) than those ratios of mixture spectra with <50% kaolinite (ratio <0.6). The differences in the band area ratios (and, therefore, the strength of the bands) were probably due to effects such as multiple scattering in the intimate (physical) mixture spectra that were not well modeled in the linear mixture spectra. Nonetheless, the linear behavior of the band area ratios indicates that using reflectance spectra to estimate the abundance of kaolinite relative to montmorillonite in binary mixtures of these two components should be possible. Additionally, because the slope of the ratios of the linear mixture spectra (SOM 16, 17) was different from the slope of the ratios of the intimate mixture

[1] Supplementary figures SOM 1–17 have been deposited with the Editor in Chief and are available at www.clays.org/JOURNAL/JournalDeposits.html

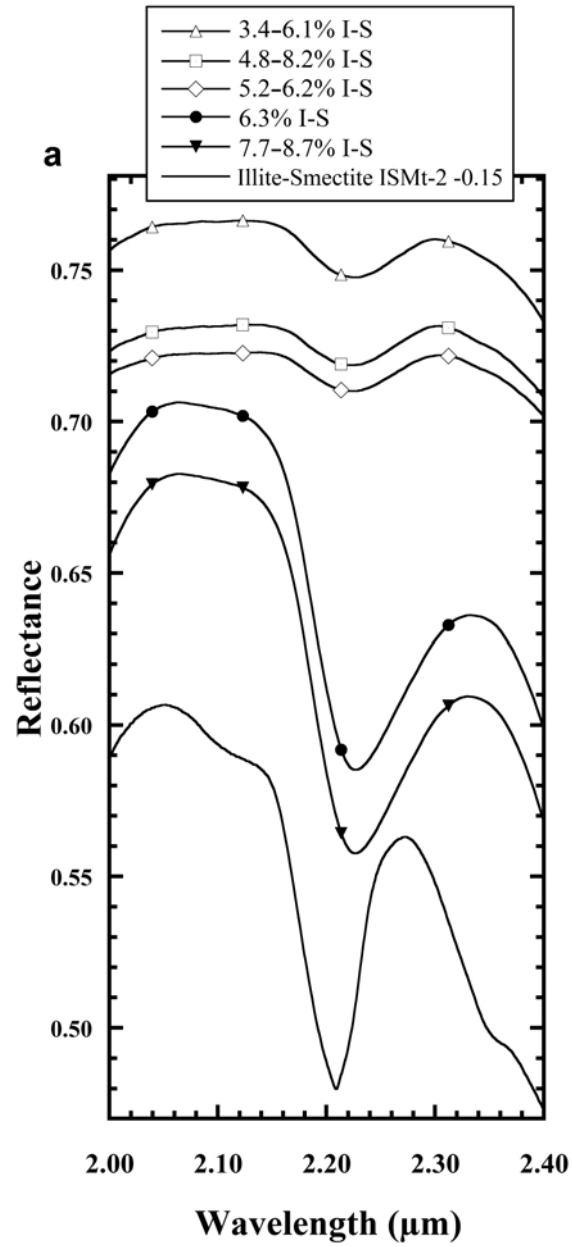

Figure 7 (*above and facing page*). Spectra of hydrothermally altered glass-I-S samples. (a) Spectra from 2.0 to 2.4 μm. At <6 wt.% I-S, the spectra resembled that of altered glass but at 6–10% I-S, the spectra begin to resemble the spectrum of I-S; however, the band is broader and occurs at 2.23 μm rather than 2.21 μm. (b) Spectra from 0.5 to 2.6 μm. In the samples with >6 wt.% I-S, features due to H_2O were detectable at 0.95 and 1.15 μm and the 1.4 and 1.9 μm features due to OH and H_2O were stronger than in the <6 wt.% I-S samples. (c) Spectra from 0.3 to 4.0 μm. The shapes of the 3 μm water bands for the <6 wt.% I-S samples were straight-sided and return to almost the same level of reflectance as at 2.5 μm. The >6 wt.% I-S samples had a broader feature and only returned to ~60 wt.% of the 2.5 μm reflectance, probably because they contained more water than the <6 wt.% I-S samples. The I-S spectrum has a sharp absorption at ~2.7 μm characteristic of smectites and a broad shoulder at 3.0 μm.

https://doi.org/10.1346/CCMN.2011.0590404 Published online by Cambridge University Press

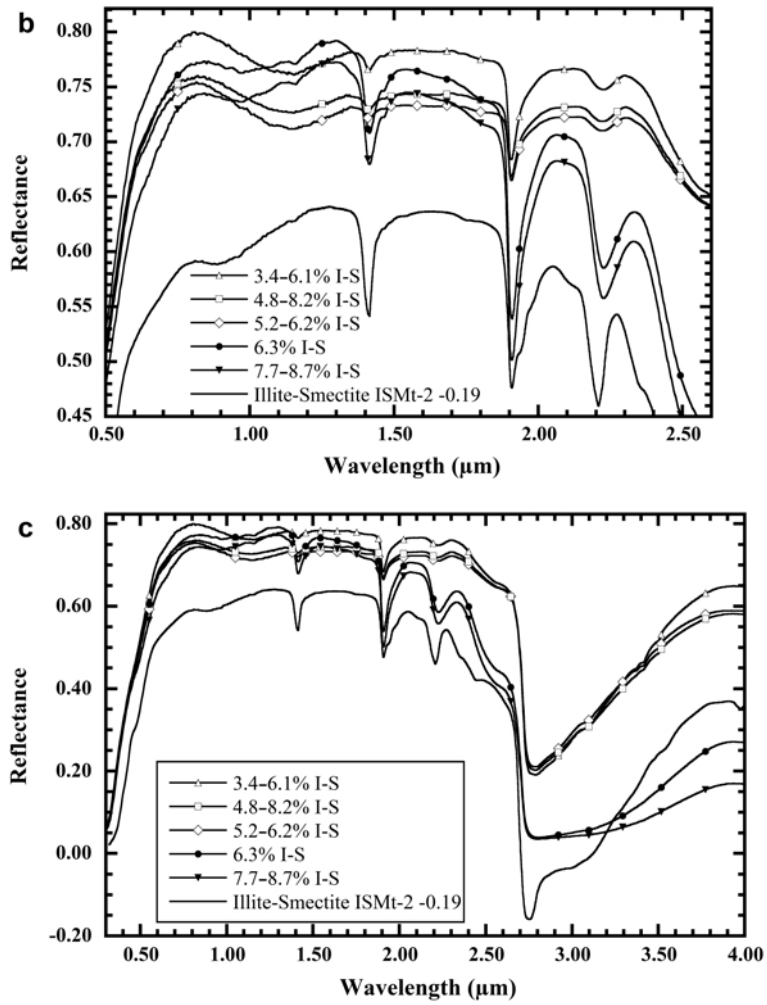

spectra (Figure 8b,c), determining whether a spectrum from Earth, Mars, or another surface is due to areal mixing or physical mixing within an outcrop should be possible.

COMPARISON WITH CRISM SPECTRA

Comparison of montmorillonite-hydrated silica mixtures

The CRISM reflectance spectra interpreted as containing montmorillonite and a form of hydrated silica most closely resemble the laboratory mixtures containing montmorillonite and obsidian (Figure 9). Performing a simple least-squares fitting, the mixture containing 50% montmorillonite and 50% obsidian most closely matches the CRISM spectrum 848D-a with an R^2 of 0.888 (Table 4). The next closest matches are 80% montmorillonite and 848D-a (R^2 = 0.877), 50% montmorillonite and 848D-c (R^2 = 0.866), and 20% montmorillonite and 848D-a (R^2 = 0.863). None of the montmorillonite-obsidian mixtures provided a particularly good match to spectrum 848D-b (all R^2 values are <0.68, Table 4). This spectrum is possibly better matched by a different form of hydrated silica, similar to spectra discussed by Milliken *et al.* (2008).

Table 3. Average band centers and standard deviation from the average for the four bands identified by MGM in kaolinite-montmorillonite mixtures.

	Band 1	Band 2	Band 3	Band 4
Average band center	2.172	2.201	2.218	2.255
Standard deviation	0.0168363	0.00584858	0.0138495	0.0277112

https://doi.org/10.1346/CCMN.2011.0590404 Published online by Cambridge University Press

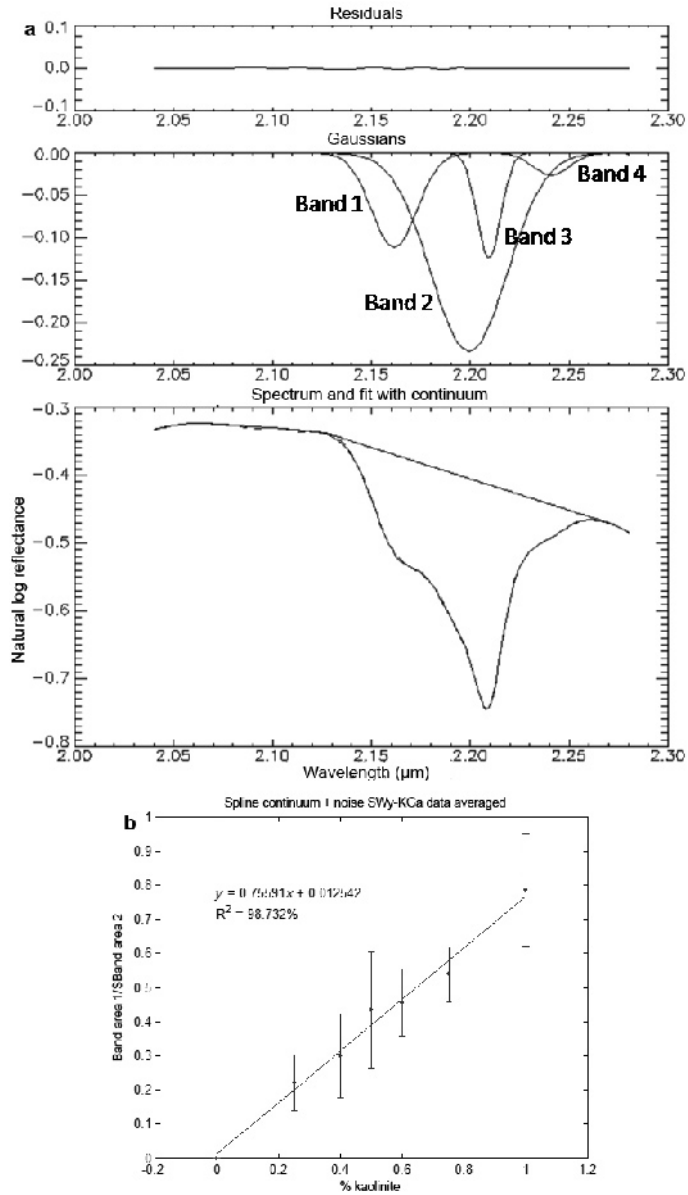

Figure 8 (*above and facing page*). (a) MGM result for 40 wt.% kaolinite-montmorillonite intimate mixture. The bottom panel shows the spectrum with the continuum and fit result (dashed line; in this case, it overlies the spectrum almost perfectly), the middle panel shows the calculated Gaussians, and the top panel plots the residuals, which are all <0.025 here. The Gaussian band numbers used for the ratio calculations are indicated. (b) From MGM, the area of band 1 (kaolinite 2.17 μm) divided by the area of band 2 (kaolinite and montmorillonite 2.20 μm) plotted against the amount of kaolinite in the sample, scaled to unity for pure kaolinite. The ratio of these areas increases linearly with the amount of kaolinite in the sample. (c) From MGM, the area of band 1 (kaolinite 2.17 μm) divided by the sum of the areas of bands 2, 3, and 4 (kaolinite and montmorillonite 2.20 μm and 2.21 μm, and montmorillonite 2.24 μm, respectively) plotted against the amount of kaolinite in the sample, scaled to unity. The ratio of these areas increased linearly with the amount of kaolinite in the sample. (d) Plot of the ratio of the area of band 1 to the area of band 2 in the kaolinite-montmorillonite intimate mixtures divided by the same ratio in the linear mixtures. In all cases, the ratio is <1, indicating that the proportional relationship of the areas is always larger in the linear mixtures than the intimate mixtures. In addition, the ratios appear to break down into two groups: the mixtures with >50% kaolinite all have ratios >0.65 and those with <50% kaolinite are <0.6, indicating that the intimate mixture spectra with >50% kaolinite behave more similarly to the linear mixture spectra than those spectra of mixtures with <50% kaolinite.

https://doi.org/10.1346/CCMN.2011.0590404 Published online by Cambridge University Press

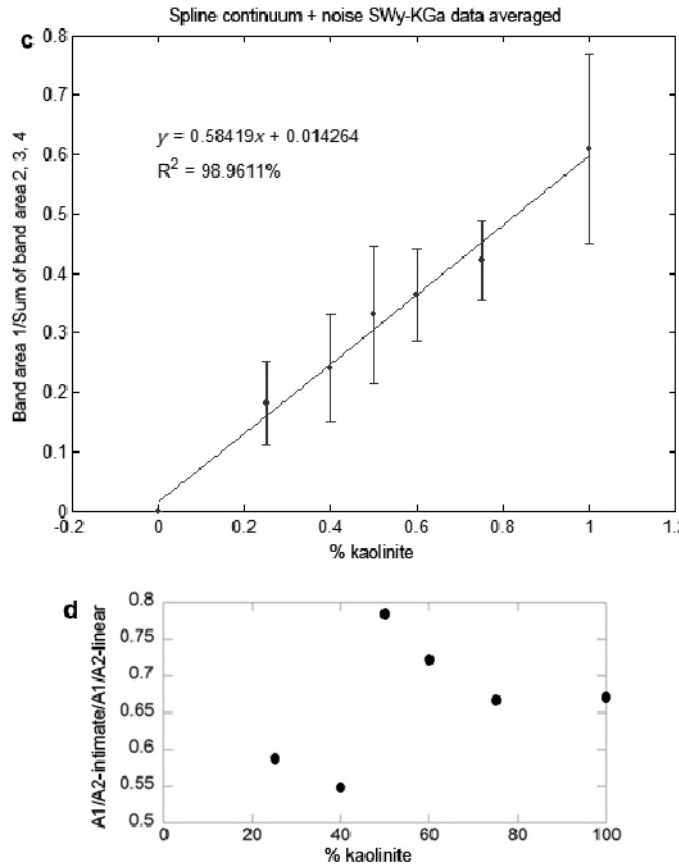

The spectra of the hydrothermally altered glass-I-S samples exhibited a ~2.2 μm absorption at a longer wavelength (2.23 μm) than the CRISM spectra (2.21 μm), although they are both broad. The spectra of the natural samples containing opal and smectite showed no broadening of the 2.21 μm band to longer wavelengths, though some broadening to shorter wavelengths was observed in the spectra of the sample containing the smallest amount of smectite (54.5%). Due to these dissimilarities, neither the glass-I-S samples nor the opal-A-smectite samples were as good a match to the CRISM spectra as the montmorillonite-obsidian samples.

Table 4. R^2 values fitting the montmorillonite-obsidian mixtures to the Mawrth Vallis CRISM spectra from 2.0 to 2.4 μm. The best match with an R^2 value of 0.888 is the 50% montmorillonite spectrum to the 848D-a spectrum.

	848D-a	848D-b	848D-c
B579	0.860	0.632	0.833
JB586-80%	0.877	0.654	0.853
JB585-50%	**0.888**	0.688	0.866
JB584-20%	0.863	0.676	0.840
JB583-10%	0.666	0.652	0.659
JB582-8%	0.653	0.637	0.645
JB581-5%	0.375	0.452	0.369
JB580-2%	0.444	0.491	0.439
JB578-obsidian	0.260	0.363	0.260

Comparison of kaolinite-bearing mixtures

For the spectra of the kaolinite mixtures, none provided a good match to the CRISM spectra that exhibited kaolinite-like features (Figure 10, Table 5). The closest match was 30% kaolinite−70% montmorillonite for spectrum 43EC-b, with an R^2 of 0.639 (Table 5). In general, the kaolinite-montmorillonite intimate mixture spectra had higher R^2 values for a given CRISM spectrum than the kaolinite-opal-A intimate mixture spectra, although the fits to the CRISM spectrum 848D-a were comparable (Table 5). Mixing kaolinite with montmorillonite broadens the band at 2.21 μm but does not reduce the band strength, unlike mixtures with opal-A or silica. The continuum across the 2.21 μm feature in CRISM data was close to flat, which is more similar to the spectra of the montmorillonite-kaolinite mixtures than those of kaolinite-opal-A, although all of the continua for the laboratory spectra were negative.

Other minerals are probably also present in the clay-bearing rocks at Mawrth Vallis, so although mixtures of

https://doi.org/10.1346/CCMN.2011.0590404 Published online by Cambridge University Press

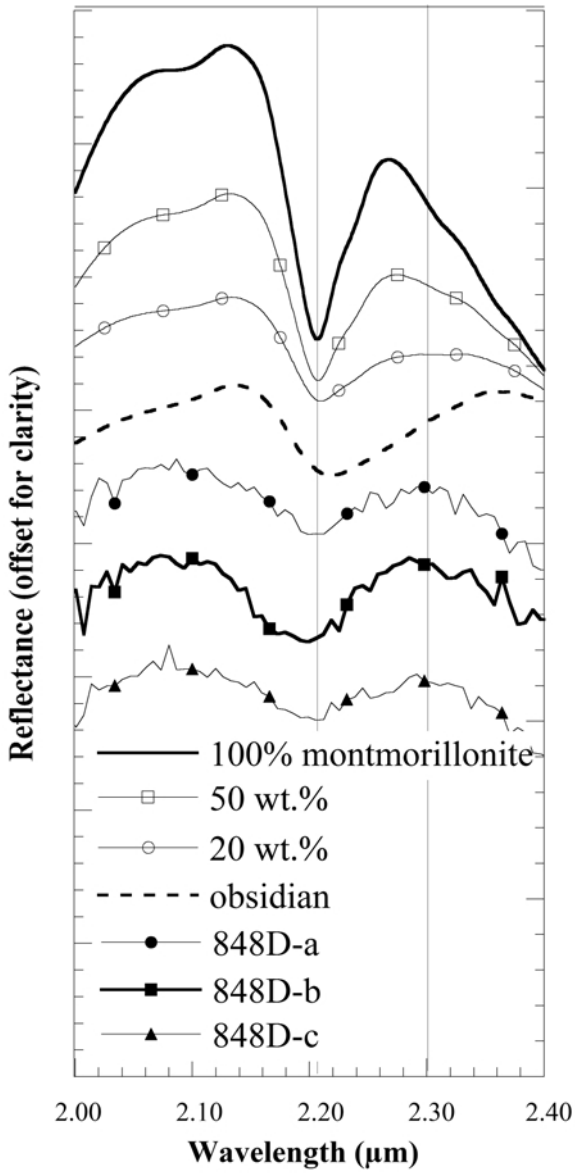

Figure 9. Spectra of select montmorillonite-obsidian mixtures compared to CRISM spectra from image FRT0000848D. The mixture with 50% montmorillonite most closely matches the shape of the CRISM spectra but this cannot be used to determine modal mineralogy.

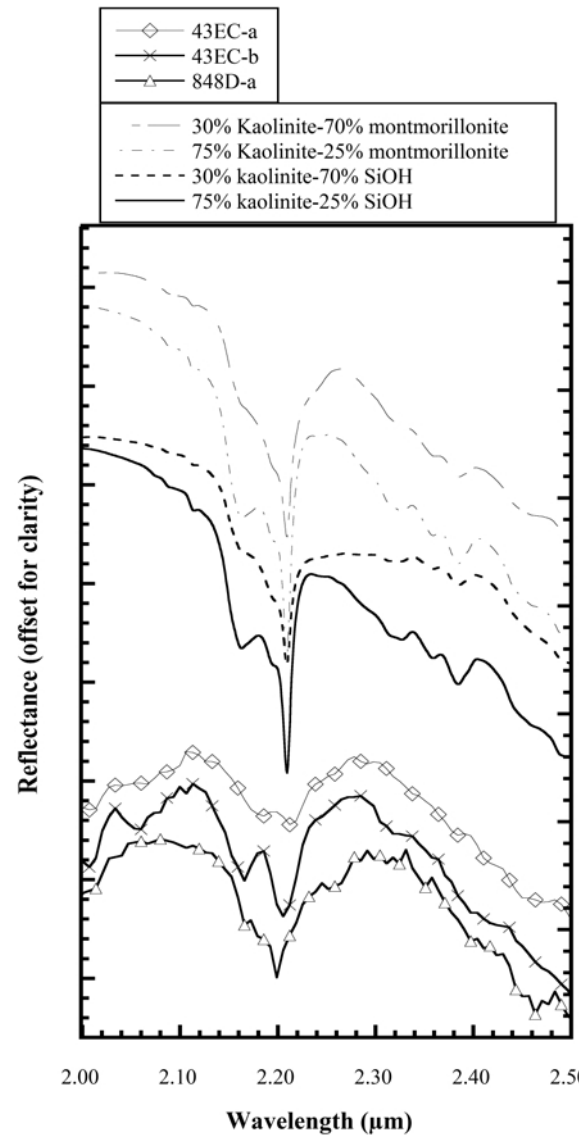

Figure 10. Spectra of kaolinite-montmorillonite and kaolinite-SiOH mixtures compared to CRISM spectra from images FRT000043EC and FRT0000848D. The 30% kaolinite mixtures most closely match the 848D spectrum and the broadened nature of the 43EC spectra. Differences in the 2.17 and 2.21 μm bands could be due to a different kaolin-family mineral such as dickite being present, rather than kaolinite.

certain minerals can be demonstrated to be more likely than others to be responsible for the observed band shape, no specific conclusions can be drawn about the weight- or volume-percent abundance of specific phases in the whole rock. Data from the Thermal Emission Spectrometer (TES, on board Mars Global Surveyor) indicate the presence of abundant plagioclase in this region (Michalski and Fergason, 2008), which is difficult to uniquely identify at VNIR wavelengths. Modeling by Poulet *et al.* (2008) also suggests the presence of ferrihydrite, minor amounts of pyroxene, and Martian dust in this region in addition to plagioclase and phyllosilicate minerals.

CONCLUSIONS

The spectra of intimate mixtures of kaolinite, montmorillonite, obsidian, and opal-A, when sieved to <125 μm, are very similar to linear (numerical) mixtures in the 0.3–2.0 μm wavelength region. In the 2.0–2.5 μm wavelength range, slight variations between intimate and linear mixture spectra were observed; the kaolinite

https://doi.org/10.1346/CCMN.2011.0590404 Published online by Cambridge University Press

Table 5. R^2 values fitting the kaolinite-montmorillonite mixtures to the Mawrth Vallis CRISM spectra from 2.0 to 2.4 μm. The best match with an R^2 value of 0.639 is the 30% kaolinite spectrum to the 43EC-a spectrum.

	43EC-a	43EC-b	848D-a
Kaolinite-montmorillonite intimate mixtures			
75% Kaolinite	0.502	0.598	0.557
60% Kaolinite	0.513	0.606	0.568
50% Kaolinite	0.538	0.623	0.589
40% Kaolinite	0.531	0.618	0.584
30% Kaolinite	0.564	**0.639**	0.610
25% Kaolinite	0.564	0.638	0.609
15% Kaolinite	0.584	0.646	0.623
Kaolinite-opal-A intimate mixtures			
75% kaolinite	0.494	0.590	0.556
50% kaolinite	0.490	0.574	0.575
40% kaolinite	0.493	0.574	0.578
30% kaolinite	0.478	0.550	0.577
25% kaolinite	0.442	0.500	0.554

absorption at 2.17 μm was stronger in intimate mixtures with montmorillonite than in equivalent numerical linear mixtures. When this and the 2.21 μm absorption were modeled using MGM, the ratio of the area of the 2.17 μm band to the 2.21 μm band was linearly proportional to the amount of kaolinite in the mixture, as was the ratio of the area of 2.17 μm band to the sum of the areas of the 2.20, 2.21, and 2.24 μm bands. In spectra of altered glass-illite-smectite mixtures, however, non-linear variation was observed in the spectral shape throughout the VNIR-SWIR wavelength region between samples with <6% I-S and those with 6–8.7% I-S.

Comparing the mixture spectra to CRISM spectra, the montmorillonite-obsidian mixtures with ~50% montmorillonite provided the closest match, whereas the montmorillonite-Kilauea silica (dominated by opal-A) mixtures provided a poorer match to the CRISM montmorillonite-like spectra. The montmorillonite-kaolinite mixtures with ~30% kaolinite are most similar to the CRISM spectra of Mawrth Vallis that exhibit some kaolinite character. The kaolinite-opal-A mixtures with 30–50% silica have a similar shape at 2.1–2.22 μm, but the band is not broadened to longer wavelengths, making it a less likely candidate. The results of this laboratory mixture study identify a variety of plausible clay/silica mixtures that could be contributing to the reflectance spectra observed by the CRISM instrument at Mawrth Vallis, Mars.

ACKNOWLEDGMENTS

Support of this study from the Mars Fundamental Research program, the MRO-CRISM mission, NASA's Graduate Student Researcher's program, and the Naval Postgraduate School in Monterey, California, is much appreciated. The authors thank T. Hiroi at RELAB for the reflectance spectra. Brown University's RELAB is supported by NASA grant NNG06GJ31G. The authors also thank E. Finley at the National Institute for Nanotechnology, National Research Council, Canada, for the spectral curve fitting to CRISM data and are grateful also to R.E. Milliken and two anonymous reviewers for their helpful comments which greatly improved this manuscript.

REFERENCES

Bibring, J.-P., Langevin, Y., Mustard, J.F., Poulet, F., Arvidson, R., Gendrin, A., Gondet, B., Mangold, N., Pinet, P., and Forget, F. (2006) Global mineralogical and aqueous Mars history derived from OMEGA/Mars Express data. *Science*, **312**, 400–404.

Bibring, J.-P., Loizeau, D., Pelkey, S.M., Murchie, S., Mustard, J.F., Bishop, J.L., Ehlmann, B.L., Gondet, B., Mangold, N., Poulet, F., Roach, L.A., and Seelos, F. (2007) Coupled OMEGA-CRISM Observations of Marwth Vallis. *Lunar and Planetary Science Conference XXXVIII*, Lunar and Planetary Institute, Houston, Texas, USA..

Bishop, J.L. and Dummel, A. (1996) The influence of fine-grained hematite powder on the spectral properties of Mars soil analogs; VIS-NIR bi-directional reflectance spectroscopy of mixtures. *Lunar and Planetary Science Conference XXVII*, Lunar and Planetary Institute, Houston, Texas, USA.

Bishop, J.L.,Pieters, C.M., and Burns, R.G. (1993) Reflectance and Mössbauer spectroscopy of ferrihydrite-montmorillonite assemblages as Mars soil analog materials. *Geochimica et Cosmochimica Acta*, **57**, 4583–4595.

Bishop, J.L., Pieters, C.M., and Edwards, J.O. (1994) Infrared spectroscopic analyses on the nature of water in montmorillonite. *Clays and Clay Minerals*, **42**, 701–715.

Bishop, J.L., Schiffman, P., Lane, M.D., and Dyar, M.D. (2005) Solfataric alteration in Hawaii as a mechanism for formation of the sulfates observed on Mars by OMEGA and the MER instruments. *Lunar and Planetary Science Conference XXXVI*, Lunar and Planetary Institute, Houston, Texas, USA.

Bishop, J.L., Lane, M.D., Dyar, M.D., and Brown, A.J. (2008a) Reflectance and emission spectroscopy study of four groups of phyllosilicates: Smectites, kaolinite-serpentines, chlorites and micas. *Clay Minerals*, **43**, 35–54.

Bishop, J.L., Noe Dobrea, E.Z., McKeown, N.K., Parente, M., Ehlmann, B.L., Michalski, J.R., Milliken, R.E., Poulet, F., Swayze, G.A., Mustard, J.F., Murchie, S.L., and Bibring, J.-P. (2008b) Phyllosilicate diversity and past aqueous activity revealed at Mawrth Vallis, Mars. *Science*, **321**, 830–833.

Burns, R.G. (1993) *Mineralogical Applications of Crystal Field Theory.* Cambridge University Press, Cambridge, UK.

Chipera, S.J. and Bish, D.L. (2001) Baseline studies of the Clay Minerals Society Source Clays: Powder X-ray diffraction analyses, *Clays and Clay Minerals*, **49**, 398–409.

Clark, R.N., King, T.V.V., Klejwa, M., and Swayze, G.A. (1990) High spectral resolution reflectance spectroscopy of minerals. *Journal of Geophysical Research*, **95**, 12653–12680.

de la Fuente, S., Cuadros, J., and Linares, J. (2000) Quantification of mixed-layer illite-smectite in glass matrices by Fourier-transform infrared spectroscopy. *Clays and Clay Minerals*, **48**, 299–303.

de la Fuente, S., Cuadros, J., and Linares, J. (2002) Early stages of volcanic tuff alteration in hydrothermal experiments: formation of mixed-layer illite-smectite. *Clays and Clay Minerals*, **50**, 578–590.

Delineau, T., Allard, T., Muller, J.-P., Barres, O., Yvon, J., and Cases, J.-M. (1994) FTIR reflectance vs. EPR studies of structural iron in kaolinites. *Clays and Clay Minerals*, **42**, 308–320.

Edgett, K.S. and Parker, T.J. (1997) Water on early Mars: Possible subaqueous sedimentary deposits covering ancient cratered terrain in western Arabia and Sinus Meridiani. *Geophysical Research Letters*, **24**, 2897–2900.

Fairén, A.G., Chevrier, V., Abramov, O., Marzo, G.A., Gavin, P., Davila, A.F., Tornabene, L.L., Bishop, J.L., Roush, T.L., Gross, C., Kneissl, T., Uceda, E.R., Dohm, J.M., Schulze-Makuch, D., Rodríguez, J.A.P., Amils, R., and McKay, C.P. (2010) Noachian and more recent phyllosilicates in impact craters on Mars. *Proceedings of the National Academy of Sciences*, **107**, 12095–12100.

Hillier, S. and Lumsdon, D.G. (2008) Distinguishing opaline silica from cristobalite in bentonites: a practical procedure and perspective based on NaOH dissolution. *Clay Minerals*, **43**, 477–486.

Loizeau, D., Mangold, N., Poulet, F., Ansan, V., Hauber, E., Bibring, J.-P., Gondet, B., Langevin, Y., Masson, P., and Neukum, G. (2010) Stratigraphy in the Mawrth Vallis region through OMEGA, HRSC color imagery and DTM. *Icarus*, **205**, 396–418.

Makarewicz, H.D., Parente, M., and Bishop, J.L. (2008) Characterizing mafic and clay components in Libya Montes, Mars, using automated Gaussian Modeling of spectral features found in MRO/CRISM Images. *AGU Fall Meeting*, Abstract # P41B1378M.

Makarewicz, H.D., Parente, M., and Bishop, J.L. (2009a) Deconvolution of VNIR spectra using modified Gaussian modeling (MGM) with automatic parameter initialization (API) applied to CRISM. *IEEE WHISPERS 2009*, *Grenoble, France*.

Makarewicz, H.D., Parente, M., and Bishop, J.L. (2009b) Determining the composition of phyllosilicates using automated Gaussian modeling of spectral features. *Lunar and Planetary Science Conference XL*, Lunar and Planetary Institute, Houston, Texas, USA.

Marzo, G.A., Davila, A.F., Tornabene, L.L., Dohm, J.M., Fairén, A.G., Gross, C., Kneissel, T., Bishop, J.L., Roush, T.L., and McKay, C.P. (2010) Evidence for Hesperian impact-induced hydrothermalism on Mars. *Icarus*, **208**, 667–683.

McKeown, N.K., Bishop, J.L., Noe Dobrea, E.Z., Parente, M., Ehlmann, B.L., Mustard, J.F., Murchie, S.L., Swayze, G.A., Bibring, J.-P., and Silver, E.A. (2009) Characterization of phyllosilicates observed in the central Mawrth Vallis region, Mars, their potential formational processes, and implications for past climate. *Journal of Geophysical Research – Planets*, **144**, E00D10.

Michaelian, K.H., Friesen, W.I., Yariv, S., and Nasser, A. (1991) Diffuse reflectance infrared spectra of kaolinite and kaolinite/alkali halide mixtures. Curve-fitting of the OH stretching region. *Canadian Journal of Chemistry*, **69**, 1786–1790.

Michalski, J.R. and Fergason, R.L. (2008) Composition and thermal inertia of the Mawrth Vallis region of Mars from TES and THEMIS data. *Icarus*, **199**, 25–48.

Michalski, J.R. and Noe Dobrea, E.Z. (2007) Evidence for a sedimentary origin of clay minerals in the Mawrth Vallis region, Mars, *Geology*, **35**, 951–954.

Milliken, R.E., Swayze, G.A., Arvidson, R.E., Bishop, J.L., Clark, R.N., Ehlmann, B.L., Green, R.O., Grotzinger, J.P., Morris, R.V., Murchie, S.L., Mustard, J.F., and Weitz, C. (2008) Opaline Silica in Young Deposits on Mars. *Geology*, **36**, 847–850.

Murchie, S., Arvidson, R., Bedini, P., Beisser, K., Bibring, J.-P., Bishop, J., Boldt, J., Cavender, P., Choo, T., Clancy, R.T., Darlington, E.H., Des Marais, D., Espiritu, R., Fort, D., Green, R., Guinness, E., Hayes, J., Hash, C., Heffernan, K., Hemmler, J., Heyler, G., Humm, D., Hutcheson, J., Izenberg, N., Lee, R., Lees, J., Lohr, D., Malaret, E., Martin, T., McGovern, J.A., McGuire, P., Morris, R., Mustard, J., Pelkey, S., Rhodes, E., Robinson, M., Roush, T., Schaefer, E., Seagrave, G., Seelos, F., Silvergate, P., Slavney, S., Smith, M., Shyong, W.-J., Strohbehn,K., Taylor, H., Thompson, P., Tossman, B., Wirzburger, M., and Wolff, M. (2007) Compact Reconnaissance Imaging Spectrometer for Mars (CRISM) on Mars Reconnaissance Orbiter (MRO). *Journal of Geophysical Research*, **112**, E05S03.

Murchie, S.L., Seelos, F.P., Hash, C.D., Humm, D.C., Malaret, E., McGovern, J.A., Seelos, K.D., Buczkowski, D.L., Morgan, M.F., Barnouin-Jha, O.S., Nair, H., Taylor, H.W., Patterson, G.W., Harvel, C.A., Mustard, J.F., Arvidson, R.E., McGuire, P., Smith, M.D., Wolff, M.J., and Titus, T.N. (2009) Compact Reconnaissance Imaging Spectrometer for Mars Investigation and Data Set from the Mars Reconnaissance Orbiter's Primay Science Phase. *Journal of Geophysical Research – Planets*, **114**, E00D07.

Mustard, J.F. and Pieters, C.M. (1989) Photometric phase functions of common geologic minerals and applications to quantitative analysis of mineral mixture reflectance spectra. *Journal of Geophysical Research*, **94**, 13619–13634.

Mustard, J.F., Murchie, S.L., Pelkey, S.M., Ehlmann, B.L., Milliken, R.E., Grant, J.A., Bibring, J.-P., Poulet, F., Bishop, J.L., Noe Dobrea, E.Z., Roach, L.A., Seelos, F., Arvidson, R.E., Wiseman, S., Green, R., Hash, C., Humm, D., Malaret, E., McGovern, J.A., Seelos, K., Clancy, R.T., Clark, R.N., Des Marais, D., Izenberg, N., Knudson, A.T., Langevin, Y., Martin, T., McGuire, P., Morris, R.V., Robinson, M., Roush, T., Smith, M., Swayze, G.A., Taylor, H., Titus, T.N., and Wolff, M. (2008) Hydrated silicate minerals on Mars observed by the Mars Reconnaissance Orbiter CRISM instrument. *Nature*, **454**, 305–309.

Nash, D.B. and Conel, J.E. (1974) Spectral reflectance systematics for mixtures of powdered hypersthene, labradorite, and ilmenite. *Journal of Geophysical Research*, **79**, 1615–1621.

Noe Dobrea, E.Z., Bishop, J.L., McKeown, N.K., Fu, R., Rossi, C.M., Michalski, J.R., Heinlein, C., Hanus, V., Poulet, F., Mustard, J.F., Murchie, S.L., McEwen, A.S., Swayze, G.A., Bibring, J.-P., Malaret, E., and Hash, C. (2010) Mineralogy and stratigraphy of phyllosilicate-bearing and dark mantling units in the greater Mawrth Vallis/west Arabia Terra area: Constraints on geological origin. *Journal of Geophysical Research – Planets*, **115**, E00D19.

Parente, M. (2008) A new approach to denoising CRISM images. *Lunar and Planetary Science Conference XXXIX*, Lunar and Planetary Institute, Houston, Texas, USA.

Parente, M., Makarewicz, H.D., and Bishop, J.L. (2011) Decomposition of mineral sbsorption bands using nonlinear least squares curve fitting: Application to Martian meteorites and CRISM data. *Planetary and Space Science*, **59**, 423–442.

Petit, S., Mádejova, J., Decarreau, A., and Martin, F. (1999) Characterization of octahedral substitutions in kaolinites using near infrared spectroscopy. *Clays and Clay Minerals*, **47**, 103–108.

Poulet, F., Bibring, J.-P., Mustard, J.F., Gendrin, A., Mangold, N., Langevin, Y., Arvidson, R.E., Gondet, B., and Gomez, C. (2005) Phyllosilicates on Mars and implications for the early Mars history. *Nature*, **438**, 632–627.

Poulet, F., Mangold, N., Loizeau, D., Bibring, J.-P., Langevin, Y., Michalski, J.R., and Gondet, B. (2008) Abundance of minerals in the phyllosilicate-rich units on Mars. *Astronomy and Astrophysics*, **487**, L41–L44.

Scott, D.H. and Tanaka, K.L. (1986) Geologic map of western equatorial region of Mars. MI, USGS: I-1802-A.

Singer, R.B. (1981) Near-infrared spectral reflectance of mineral mixtures: Systematic combinations of pyroxenes,

olivine, and iron oxides. *Journal of Geophysical Research*, **86**, 7967–7982.

Sunshine, J.M. and Pieters, C.M. (1993) Estimating modal abundances from the spectra of natural and laboratory pyroxene mixtures using the Modified Gaussian Model. *Journal of Geophysical Research*, **98**, 9075–9087.

Sunshine, J.M., Pieters, C.M., and Pratt, S.F. (1990) Deconvolution of mineral absorption bands: An improved approach. *Journal of Geophysical Research*, **95**, 6955–6966.

Wray, J.J., Ehlmann, B.L., Squyres, S.W., Mustard, J.F., and Kirk, R.L. (2008) Compositional stratigraphy of clay-bearing layered deposits at Mawrth Vallis, Mars. *Geophysical Research Letters*, **35**, L12202.

(*Received 10 May 2010; revised 27 September 2011; Ms. 437; A.E. R. Milliken*)